VIIRS On-Orbit Calibration for Ocean Color Data Processing

Robert E. Eplee, Jr.,[a] Kevin R. Turpie,[a] Gwyn F. Fireman,[a]
Gerhard Meister,[b] Thomas C. Stone,[c], Frederick S. Patt,[a]
Bryan A. Franz,[b] Sean W. Bailey,[d] Wayne D. Robinson,[a]
and Charles R. McClain[b]

[a]Science Applications International Corporation, Beltsville, Maryland 20705, USA
[b]NASA Goddard Space Flight Center, Greenbelt, Maryland 20771, USA
[c]US Geological Survey, Flagstaff, Arizona 86001, USA
[d]FutureTech Corporation, Greenbelt, Maryland 20770, USA

ABSTRACT

The NASA VIIRS Ocean Science Team (VOST) has the task of evaluating Suomi NPP VIIRS ocean color data for the continuity of the NASA ocean color climate data records. The generation of science quality ocean color data products requires an instrument calibration that is stable over time. Since the VIIRS NIR Degradation Anomaly directly impacts the bands used for atmospheric correction of the ocean color data (Bands M6 and M7), the VOST has adapted the VIIRS on-orbit calibration approach to meet the ocean science requirements. The solar diffuser calibration time series and the solar diffuser stability monitor time series have been used to derive changes in the instrument response and diffuser reflectance over time for bands M1–M11. The lunar calibration observations have been used, in cooperation with the USGS ROLO Program, to derive changes in the instrument response over time for these same bands. In addition, the solar diffuser data have been used to develop detector-dependent striping and mirror side-dependent banding corrections for the ocean color data. An ocean surface reflectance model has been used to perform a preliminary vicarious calibration of the VIIRS ocean color data products. These on-orbit calibration techniques have allowed the VOST to produce an optimum time-dependent radiometric calibration that is currently being used by the NASA Ocean PEATE for its VIIRS ocean color data quality evaluations. This paper provides an assessment of the current VIIRS radiometric calibration for the ocean color data products and discusses the path forward for improving the quality of the calibration.

Keywords: VIIRS, solar calibration, lunar calibration, vicarious calibration, radiometric stability

1. INTRODUCTION

The Suomi National Polar-orbiting Partnership (NPP) Visible Infrared Imaging Radiometer Suite (VIIRS) was launched into an 824-km sun-synchronous polar orbit with a node of 13:30 pm on October 28, 2012. VIIRS acquired its first image when the nadir door of the instrument was opened on November 21, 2011. The instrument's cooled focal planes were turned on January 20, 2012. VIIRS is a 22-band scanning filter radiometer whose design heritage is SeaWiFS (rotating telescope with half-angle mirror) and MODIS (solar diffuser, solar diffuser screen, solar diffuser stability monitor). This paper discusses on-orbit calibration of the VIIRS reflective solar bands (whose characteristics are listed in Table 1). The primary calibration responsibility resides with the NOAA NESDIS/STAR VIIRS Sensor Data Record (SDR) Calibration Working Group (CWG). Since production of climate quality ocean color data products places stringent requirements on the on-orbit calibration of the reflective solar bands[1] (see Fig. 1), the NASA VIIRS Ocean Science Team (VOST) is implementing an in-house VIIRS on-orbit calibration capability in order to meet those requirements. This effort is being carried out in cooperation with the NESDIS/STAR SDR CWG, the NASA VIIRS Characterization Support Team (VCST), and the USGS Robotic Lunar Observatory (ROLO) program. This paper presents the current status of the VOST calibration efforts.

Table 1. **VIIRS Reflective Solar Bands.** The SWIR focal plane was not turned on until January 20, 2012. This paper addresses the calibration of the M bands.

Band	Band Center (nm)	Bandwidth (nm)	Single/Dual Gain	Spatial Resolution at Nadir (m)	Focal Plane
M1	412	20	DG	750	VNIR
M2	445	18	DG	750	VNIR
M3	488	20	DG	750	VNIR
M4	555	20	DG	750	VNIR
I1	640	80	SG	375	VNIR
M5	672	20	DG	750	VNIR
M6	746	15	SG	750	VNIR
I2	865	41	SG	375	VNIR
M7	865	41	DG	750	VNIR
M8	1240	20	SG	750	SWIR
M9	1378	15	SG	750	SWIR
I3	1610	60	SG	375	SWIR
M10	1610	60	SG	750	SWIR
M11	2250	50	SG	750	SWIR

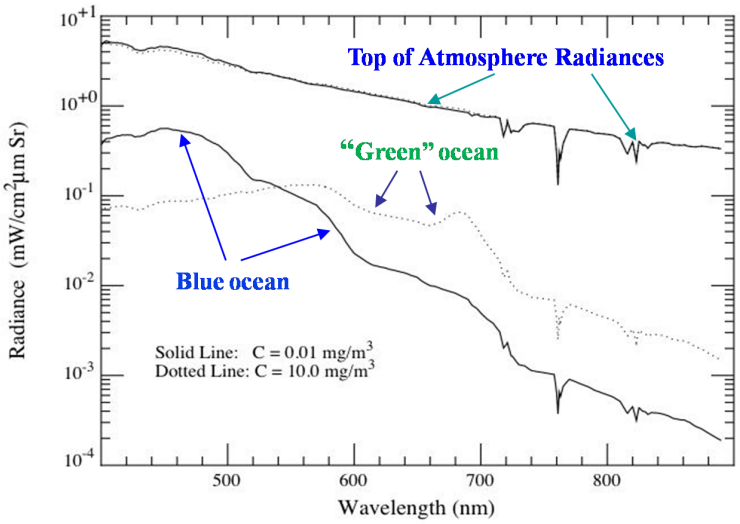

Figure 1. **VIIRS Atmospheric Correction Rationale.** Atmospheric correction removes > 85% of the signal from the top-of-the-atmosphere radiances, so a 0.1% calibration error in the TOA radiances will introduce an error of sin 0.1% in the water-leaving radiances.

Early in the VIIRS on-orbit operations, the Near-Infrared Degradation Anomaly was observed, where tungsten oxide contamination of mirrors in the rotating telescope assembly was found to be causing a rapid decrease in mirror reflectance for the near infrared spectral region.[2] The operational configuration of VIIRS was changed frequently while the anomaly was under investigation. Normal operation of the instrument began on January 2 in preparation for the first lunar calibration, and the instrument performance has essentially been stable since that time. The VOST on-orbit calibration analyses focus on data collected since the start of normal operations on January 2.

Currently, solar calibration is the primary method of monitoring the on-orbit radiometric performance of the reflective solar bands. The VIIRS solar diffuser is a Spectralon panel placed behind a solar attenuation screen with $\sim 13\%$ transmission. VIIRS observes sunlight reflected by the solar diffuser (SD) once per orbit as the spacecraft crosses the North Pole, moving from the Earth's shadow into sunlight. The change in radiometric sensitivity over time is computed from the solar diffuser data (the F-factor). Contemporaneously, the solar diffuser stability monitor (SDSM) is simultaneously observing the sun and the solar diffuser to monitor changes in the diffuser BRDF over time (the H-factor). The SDSM is an 8-channel radiometer with wavelengths corresponding to VIIRS bands M1–M7 and a reference channel at 935 nm. The SDSM views the solar diffuser directly and views the Sun through an attenuation screen that has $\sim 95\%$ transmission. The solar diffuser time series must be corrected by the SDSM-derived BRDF change to yield the actual change in instrument response. This solar calibration method yields a calibration of the instrument on a per-band, per-detector basis for the two gain states and the two mirror sides.

Lunar calibration is the secondary method of monitoring the radiometric response of the reflective solar bands on orbit. The spacecraft is rolled once per month to observe the Moon at a nominal phase angle of 51°. The resulting integrated lunar irradiances are processed by the USGS Robotic Lunar Observatory (ROLO) photometric model of the Moon[3,4] to yield the time series of lunar residuals (the radiometric response over time). The relative trends in radiometric response for VIIRS in the lunar data and solar data are generally in agreement. Currently, the lunar data is being used to validate the radiometric trends observed in the solar calibrations. As more lunar calibration data become available the lunar time series may supplement or supplant the solar calibration data as the primary radiometric monitor.

Vicarious calibration of VIIRS allows the VOST to adjust the on-orbit calibration of the instrument to match the system-level calibration of the Marine Optic Buoy (MOBY)[5,6] and the VIIRS atmospheric correction algorithm. The vicarious calibration mitigates uncertainties (e.g., biases) in the spectral calibration of VIIRS, the calibration of the MOBY, and the atmospheric correction algorithm.[7] It normally takes a year of on-orbit operations to acquire a sufficient number of satellite/*in situ* matchups for a robust vicarious calibration. Accordingly, the VOST has performed the initial vicarious calibration of VIIRS against an ocean surface reflectance model.[8]

2. SOLAR CALIBRATION

VIIRS views the Sun reflecting off of the solar diffuser as the NPP spacecraft passes over the North Pole, moving from the Earth's shadow into sunlight. Fig. 2 shows a radiance profile across the diffuser during a typical solar calibration, along with the radiance profile observed by the solar diffuser stability monitor for the same calibration. VIIRS solar diffuser observations provide the monitor of the radiometric response of the instrument over time. The ratio of the SDSM solar diffuser observations to the SDSM observations of the Sun provide the monitor of the diffuser BRDF.

2.1 Solar Diffuser Stability Monitor Trends

The Solar Diffuser Stability Monitor performs its measurements in a three scan cycle: it measures the dark count by observing the space view, it measures the solar radiance reflected by the diffuser, then it measures the solar radiance directly through the SDSM screen. The BRDF trends are computed from the SDSM measurements as follows:

Further author information:
R.E.E.: Robert.E.Eplee@nasa.gov, 301 286 0953

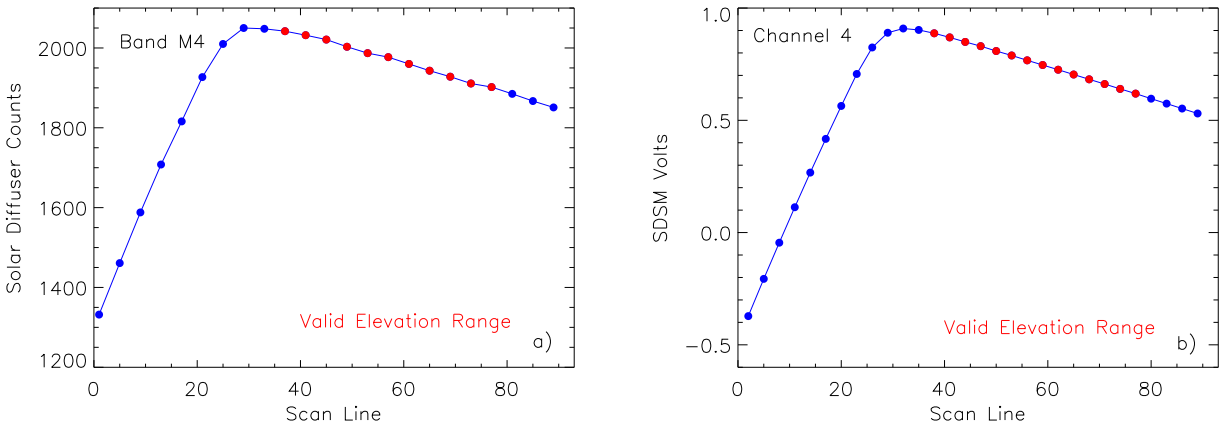

Figure 2. **Solar Diffuser Calibration Profile.** a) VIIRS band M4 profile in diffuser counts. b) SDSM channel 4 profile in SDSM volts. Red data points occur within the range of elevation angles where the BRDF of the diffuser and the transmission function of the solar diffuser and the SDSM screens were measured. Observations for each calibration are averaged over these valid scans.

The signal measured by the SDSM from the solar diffuser is a function of instrument counts:

$$DC_{sd}(\lambda,t) \;=\; \frac{dc_{sd}(\lambda,t)\;\cos(\phi(t))}{\tau_{sds}(\lambda)\,BRDF(\lambda,t)\,\Omega_{sdsm}} \tag{1}$$

where dark-subtracted Solar Diffuser counts are defined as:

$$dn_{sd}(\lambda,t) \;=\; DN_{sd}(\lambda,t) \;-\; DN_{sv}(\lambda,t) \tag{2}$$

where:

BRDF	$\equiv$	BRDF of the solar diffuser
λ	$\equiv$	VIIRS band
t	$\equiv$	time of the observation
ϕ	$\equiv$	incidence angle of the Sun on the solar diffuser
τ_{sds}	$\equiv$	transmittance of the solar diffuser screen
Ω_{sdsm}	$\equiv$	cone angle of the SDSM view of the solar diffuser
DN_{sd}	$\equiv$	solar diffuser counts
DN_{sv}	$\equiv$	space view counts.

This equation corrects the solar radiance for the attenuation by the solar diffuser screen and for the BRDF of the diffuser.

The signal measured by the SDSM from the sun through the SDSM screen is also a function of counts:

$$DC_{sun}(\lambda,t) \;=\; \frac{dc_{sun}(\lambda,t)}{\tau_{sdsm}(\lambda)} \tag{3}$$

where $\tau_{sdsm}(\lambda)$ is the transmittance of the SDSM screen. The dark-subtracted SDSM counts are defined as above. This equation corrects the solar radiance for the attenuation by the SDSM screen.

The BRDF history function is the ratio of the solar diffuser measurement to the direct solar measurement:

$$h(\lambda,t) \;=\; \frac{DC_{sd}(\lambda,t)}{DC_{sun}(\lambda,t)} \;=\; \frac{dc_{sd}(\lambda,t)\;\cos(\phi(t))\,\tau_{sdsm}(\lambda)}{dc_{sun}(\lambda,t)\,\tau_{sds}(\lambda)\,BRDF(\lambda,t_o)\,\Omega_{sdsm}} \tag{4}$$

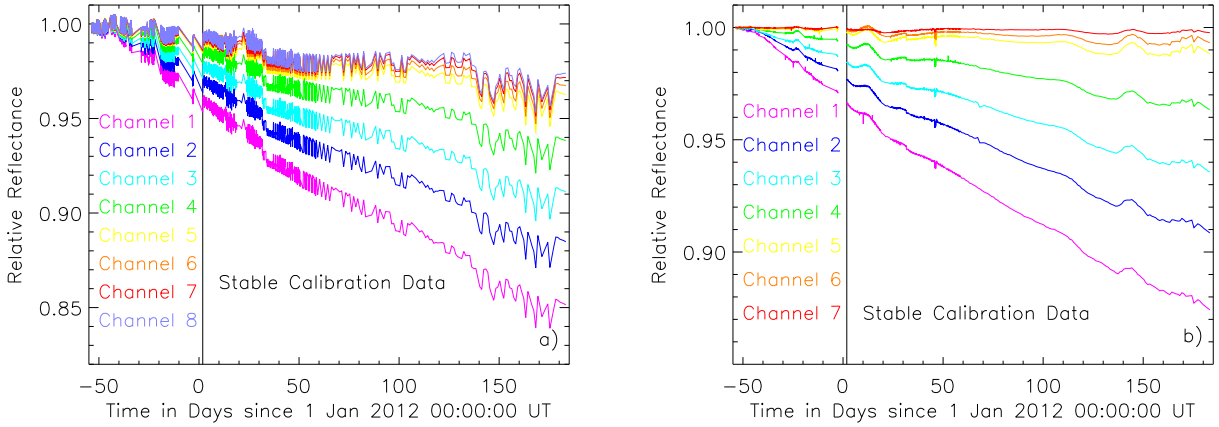

Figure 3. **Solar Diffuser Stability Monitor Time Series.** a) SDSM trends for channels 1–8. b) Normalized trends for channels 1-7. The normalized series shows the change in diffuser BRDF over time.

where t_o is the reference time for the instrument trends. The time-dependent BRDF is:

$$BRDF(\lambda,t) \;=\; BRDF(\lambda,t_o)\,\frac{h(\lambda,t)}{h(\lambda,t_0)} \tag{5}$$

so the time-dependent BRDF correction, the H-factor, is:

$$H(\lambda,t) \;=\; \frac{h(\lambda,t)}{h(\lambda,t_0)} \tag{6}$$

The SDSM trends over time are subject to measurement noise and other instrumental artifacts. The diffuser BRDF is assumed to be invariant at 935 nm, so the SDSM reference channel at 935 nm is used to normalize the SDSM trends for these artifacts. The SDSM time series for channels 1–7, normalized by the reference channel, are used to correct the band M1–M7 F-factors for changes in the diffuser BRDF. Fig. 3 shows the SDSM trends. The systematic noise in the SDSM trends is corrected for the normalized time series. The BRDF degradation decreases with increasing wavelength, as is expected. The normalization removes the systematic noise and smooths the trends over the mission. Residual noise in the the trends has led the VOST to perform linear fits to the trends and to use these fits as the H-factor corrections that are applied to the F-factors. For Channel 1, two piecewise linear fits are applied to the time series, with the break point at the start of normal operations on January 2. For Channels 2–7 a single linear fit is computed over the mission.

2.2 Solar Diffuser Trends

The calibrated radiance measured by VIIRS is:

$$L_{ev}(\lambda,t) \;=\; F(\lambda,t)\;\big(c_0(\lambda,t) \;+\; c_1(\lambda,t)\,dn_{ev}(\lambda,t) \;+\; c_2(\lambda,t)\,dn^2_{ev}(\lambda,t)\big) \tag{7}$$

where the dark-subtracted Earth View counts are defined as:

$$dn_{ev}(\lambda,t) \;=\; DN_{ev}(\lambda,t) \;-\; DN_{sv}(\lambda,t) \tag{8}$$

where:

DN_{ev}	$\equiv$	Earth View counts
DN_{sv}	$\equiv$	space view counts
F	$\equiv$	radiometric gain over time
c_i	$\equiv$	coefficients in the counts-to-radiance conversion.

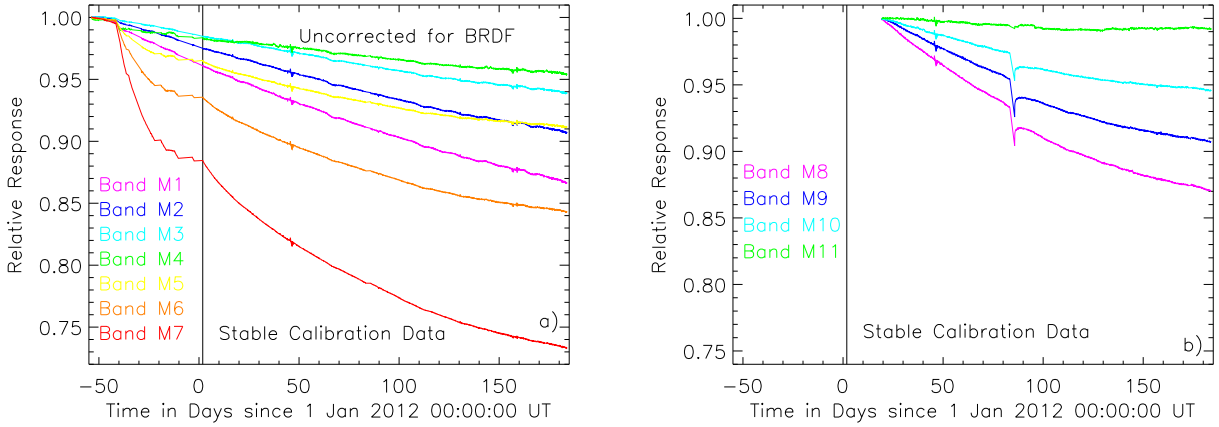

Figure 4. **Solar Diffuser Time Series.** a) The series for bands M1–M7, uncorrected for diffuser BRDF drift. b) The series for SWIR bands M8–M11.

Accordingly, the VIIRS radiometric gain over time (the F-factor) is computed from the predicted solar irradiance incident on the diffuser and the measured radiance reflected by the diffuser:

$$F(\lambda,t) \;=\; RVS(\theta_{sd},\lambda)\;\cos(\phi(t))\;\frac{L_{pred}(\lambda,t)}{L_{sd}(\lambda,t)} \tag{9}$$

where:

RVS	$\equiv$	Response vs Scan angle correction
θ_{sd}	$\equiv$	angle of incidence of the solar diffuser on the half angle mirror
ϕ	$\equiv$	incidence angle of the Sun on the solar diffuser.

The measured radiance is

$$L_{sd}(\lambda,t) \;=\; c_0(\lambda,t) \;+\; c_1(\lambda,t)\,dn_{sd}(\lambda,t) \;+\; c_2(\lambda,t)\,dn^2_{sd}(\lambda,t) \tag{10}$$

while the predicted irradiance is computed from the spacecraft geometry as:

$$L_{pred}(\lambda,t) \;=\; \frac{E_{sun}(\lambda)}{R^2_{se}(t)}\;\tau_{sds}(\lambda)\,BRDF(\lambda,to)\,H(\lambda,t) \tag{11}$$

where:

R_{se}	$\equiv$	Sun-Earth distance
E_{sun}	$\equiv$	solar irradiance

Accordingly, the F-factor becomes:

$$F(\lambda,t) \;=\; \frac{E_{sun}(\lambda)}{R^2_{se}(t)}\;\frac{RVS(\theta_{sd},\lambda)\;\cos(\phi(t))\tau_{sds}(\lambda)\,BRDF(\lambda,to)}{c_0(\lambda,t) \;+\; c_1(\lambda,t)\,dn_{sd}(\lambda,t) \;+\; c_2(\lambda,t)\,dn^2_{sd}(\lambda,t)}\;H(\lambda,t) \tag{12}$$

The inverse of the F-factor times series is the radiometric response over time.

While solar calibrations could be used to compute an absolute calibration for VIIRS using this equation, uncertainties in the diffuser characterization have limited their use to computing the relative change in the radiometric response of VIIRS over time. This relative calibration does not provide any information about the band-to-band or spectral calibration of VIIRS. The VOST will perform the spectral calibration through vicarious calibration of the ocean data.

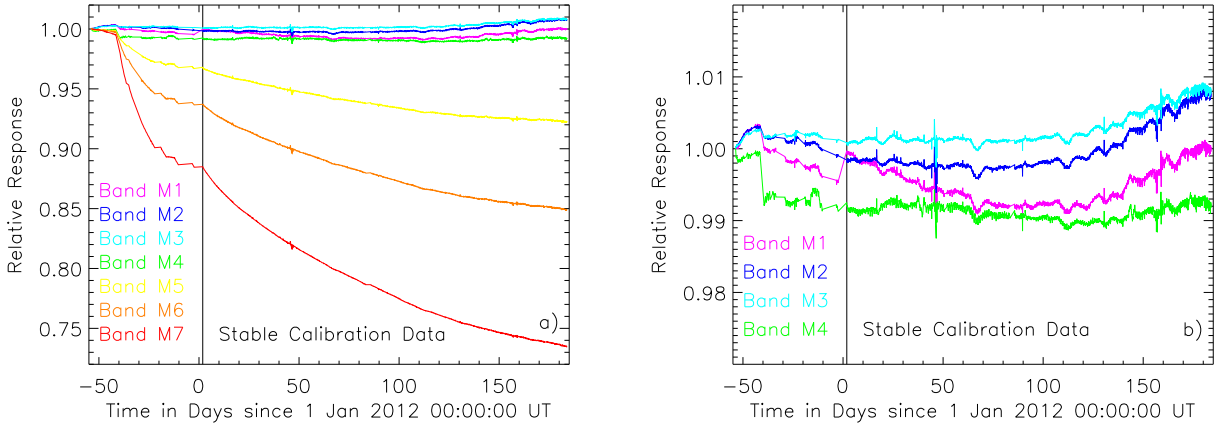

Figure 5. **Corrected Solar Diffuser Time Series.** a) The series for bands M1–M7, corrected for diffuser BRDF drift. b) The series for bands M1–M4, corrected for diffuser BRDF drift. Bands M1–M3 are over-corrected for the BRDF drift.

Fig. 4 and Fig. 5 show the radiometric response trends for VIIRS. The first set of plots shows trends without the time-dependent BRDF correction, while the second set shows trends with the time-dependent BRDF corrections applied. The bands which are subject to the near infrared degradation anomaly have small BRDF corrections, while the bands that show little response degradation (the blue bands) have significant BRDF corrections. The corrected time series for bands M1–M3 show increases in response over the latter part of the mission, which imply that the time-dependent BRDF corrections may be too large. For example, the F-factor for band M1 shows a response of $\sim 13.5\%$ at day 180 and a BRDF correction of 12.5%. The corrected F-factor time series shows an increase in response of $\sim 0.5\%$, which implies that the BRDF correction for band M1 is too large. The largest source uncertainty in the band M1 calibration is that most of the change in the F-factor is due to the diffuser BRDF and not to the instrument response. The same observation holds true for bands M2 and M3. Uncertainty in the solar diffuser BRDF over time is the predominant source of uncertainty in solar diffuser calibrations. The VOST plans to decrease this uncertainty by incorporating lunar calibrations into the VIIRS radiometric response trending.

The F-factor lookup tables that the VOST provides to the Ocean PEATE for VIIRS ocean color data processing are computed from the BRDF-corrected F-factors. Fig. 5 shows the F-factors, which are computed for each orbit (there are $\sim$ 14 orbits per day), smoothed by a 15-point Lee filter, then spline-interpolated to a single value per day. These smoothed, interpolated F-Factors are incorporated into the production F-factor lookup tables.

3. LUNAR CALIBRATION

The VIIRS lunar calibration methodology stems from MODIS heritage in that on an approximately monthly basis the NPP spacecraft is rolled to observe the Moon at a target phase angle through the space view sector.[9] One difference from MODIS is that the VIIRS instrument design forces lunar observations to be obtained while the spacecraft is in the sunlight. Accordingly, thermal exclusion zones on the spacecraft attitude limit lunar roll angles to 14° or less. The VIIRS methodology for observing the Moon has evolved to meet the on-orbit performance of the spacecraft:

1) The initial target phase angle has been adjusted from 55° to 51° to meet the exclusion zone requirements.

2) The initial set of observations were made using the space view sector of the scan line data collection. VIIRS bands are not co-registered in the space view sector, so the size of the VIIRS visible/near infrared and short wave infrared focal planes, compared to the 48 sample angular extent of the space view, prevent all of the reflective solar bands from being observed in the space view at a single roll angle.

Table 2. **Lunar Calibrations.** The VIIRS lunar calibrations obtained through May 2012. [a]The SWIR bands were still turned off on January 4.

Cal Date	Cal Type	Bands	Gains	Mirror Sides
Jan 4[a]	Roll	M4–M7	hi,lo	0,1
Jan 5	Serendipitous	M1–M3	hi,lo	0,1
Feb 3	Roll	M6, M8–M11	hi,lo	0,1
Feb 3	Roll	M1–M5, M7	hi,lo	0,1
Mar 4	Serendipitous	M3, M5–M11	hi,lo	0,1
Apr 2	Roll / Sector	M1–M11	hi	0,1
May 2	Roll / Sector	M1–M11	hi	0,1
May 21	Roll / Sector	M1–M11	hi	0,1

3) The first alternative approach to observing the Moon with all 14 reflective solar bands was to perform lunar roll maneuvers on two successive orbits at roll angles selected to target different sides of the focal planes. The drawback to this approach is the operational impact of doubling the number of spacecraft maneuvers.

4) The second alternative approach was to perform a shift of the scan line data collection so that the earth view sector, where band co-registration takes place, was rotated to cover the space view. This approach allowed all 14 solar reflective bands to view the Moon during a single lunar roll maneuver. Normally, the earth view sector allows the detector gain to be set automatically by the pixel brightness. To avoid lunar images with pixels in mixed gain states, the instrument is commanded to fixed high gain. This lunar calibration approach will be continued for the foreseeable future.

As was the case with MODIS, the Moon occasionally moves through the space view as the spacecraft/Moon geometries coincide, though the phase angle at these times is larger than the target phase angle. The VOST uses these serendipitous lunar observations to supplement planned calibrations as needed. The shortcoming to the VIIRS lunar calibration strategy is the for approximately three months out of the year (usually during the summer) the Moon is below the Earth's horizon during the lunar calibration opportunities.[9] The next NPP VIIRS lunar calibration opportunity will be in October 2012. Table 2 provides the lunar calibrations obtained so far by VIIRS and used in this analysis.

During a typical lunar maneuver, the spacecraft is first rolled to observe the Moon at the target phase angle, the Moon drifts through the space view sector due to orbital motion of the spacecraft, then the spacecraft is rolled back to nadir. Fig. 6 shows the sequence of lunar images observed by band M4 during the May 2 lunar calibration. The single gain bands are aggregated on orbit; at nadir the data from the single gain bands undergo a 3:1 aggregation along scan. The aggregation affects band M6, M8–M11, and the I bands. Fig. 6 also shows typical lunar images from the rotated earth view sector for bands M4 (unaggregated) and M6 (aggregated).

The ROLO model of the Moon requires disk-integrated lunar irradiances as input. Consequently, the VOST only uses full-disk images from the lunar calibration image sequence in computing band-averaged disk-integrated irradiances for each gain and mirror side for the calibration. The along-scan aggregation of the single-gain bands is incorporated into the oversampling correction applied to the lunar irradiances which are input to the ROLO model.

The VOST uses the ROLO model to normalize the lunar calibration time series for variations in observing geometry: Instrument/Moon distances, Sun/Moon distances, phase and libration angles. The ROLO model predicts the reflectances of the Moon based on the phase and libration angles of the observation, computes the solar irradiances for the specified instrument bands, converts the lunar reflectances to irradiances using the solar irradiances, then uses the time of the observation and the position of the spacecraft to normalize the lunar

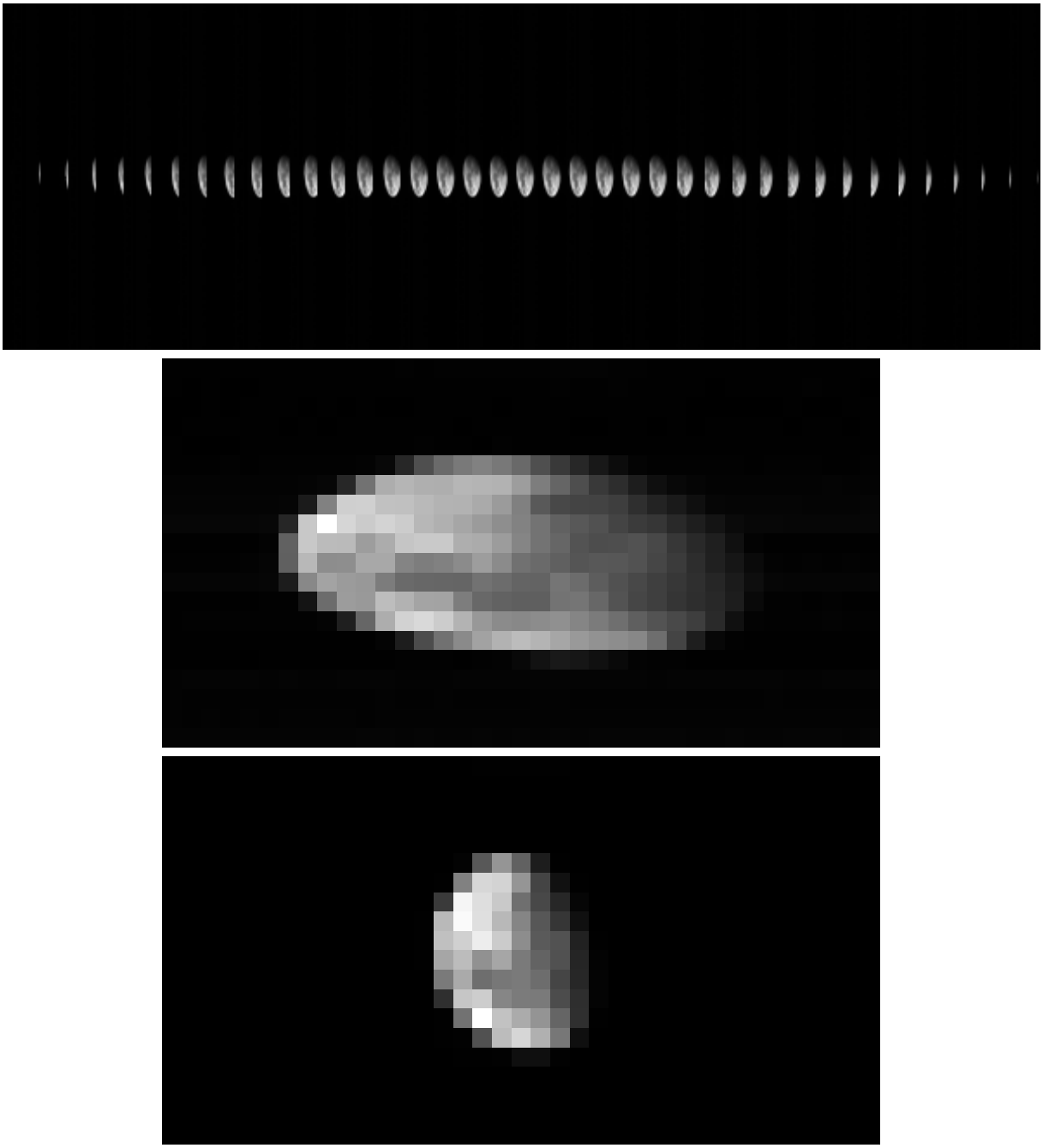

Figure 6. **Lunar Calibration Image Sequence.** a) Band M4 lunar sequence. b) Band M4 unaggregated full disk image. c) Band M6 aggregated full disk image.

irradiances to the values as seen by the instrument. The radiometric output of the model is the residual of the instrument measurement and model prediction:

$$P(\lambda,t) \;=\; \frac{K_d(t)}{A_{moon}(\lambda)}\,\frac{E_{Inst}(\lambda,t)}{E_{sun}(\lambda)} \;-\; 1 \;=\; \frac{E_{inst}(r,\lambda,t)}{E_{rolo}(r,\lambda,t)} \;-\; 1 \tag{13}$$

where:

A_{Moon}	$\equiv$	lunar reflectance predicted by the ROLO model
E_{Sun}	$\equiv$	solar irradiance
E_{rolo}	$\equiv$	lunar irradiance predicted by the ROLO model
K_d	$\equiv$	distance corrections.

The distance corrections are given by:

$$K_d(r,t) \;=\; \left(\frac{R_{sun-moon}(r,t)}{AU}\right)^2 \left(\frac{R_{inst-moon}(r,t)}{MLD}\right)^2 \tag{14}$$

where

$R_{sun-moon}$	$\equiv$	Sun – Moon distance
$R_{inst-moon}$	$\equiv$	Instrument – Moon distance
AU	$\equiv$	Astronomical Unit
MLD	$\equiv$	mean Earth – Moon distance = 384401 km

Instrument irradiance is computed from the instrument radiance and the instantaneous field of view (IFOV) of the instrument:

$$E_{inst}(\lambda,t) \;=\; IFOV_{along-scan}\, IFOV_{along-track}\; L_T(\lambda,t) \tag{15}$$

$IFOV_{along-scan}$	$\equiv$	0.3104 mrad for dual-gain M bands
$IFOV_{along-scan}$	$\equiv$	0.9313 mrads for single-gain M bands in the 3:1 aggregation zone near nadir
$IFOV_{along-track}$	$\equiv$	0.9313 mrad for all bands
L_T	$\equiv$	the disk-integrated lunar radiance.

The VIIRS radiometric response over time, as computed from the ROLO residuals, is:

$$\frac{E_{inst}(\lambda,t)}{E_{rolo}(\lambda)} \;=\; P(\lambda,t) \;+\; 1. \tag{16}$$

Fig. 7 shows the relative responses normalized to the first lunar calibration.-

Fig. 7 shows the VIIRS lunar calibration time series for bands M1–M7. Bands M5–M7 show the Near Infrared Degradation Anomaly. Band M1 shows the expected response degradation due to yellowing of the mirrors. Bands M2–M4 show little change in response to date. Comparison of the radiometric response over time derive from the lunar calibrations with the response derived from the solar calibrations is the topic of the next section.

3.1 Solar / Lunar Comparisons

Solar calibrations are performed once per orbit, while the lunar calibrations are performed once per month. Accordingly, for the initial comparison of the on-orbit solar and lunar calibrations of VIIRS, the solar-derived response trends are the baseline observations and the lunar trends are the validation of the baseline observations. These comparisons were performed for band-averaged radiances of the lunar time series and for detector 8 radiances of solar time series. For the comparisons, the first calibration in the lunar time series was normalized to the value of the solar-derived instrument response at the time of the lunar calibration. The comparisons show the agreement between the relative changes in response over time between the lunar and solar calibration time series. F-factors used in the comparison had the SDSM-derived BRDF corrections applied. Fig. 8 shows this

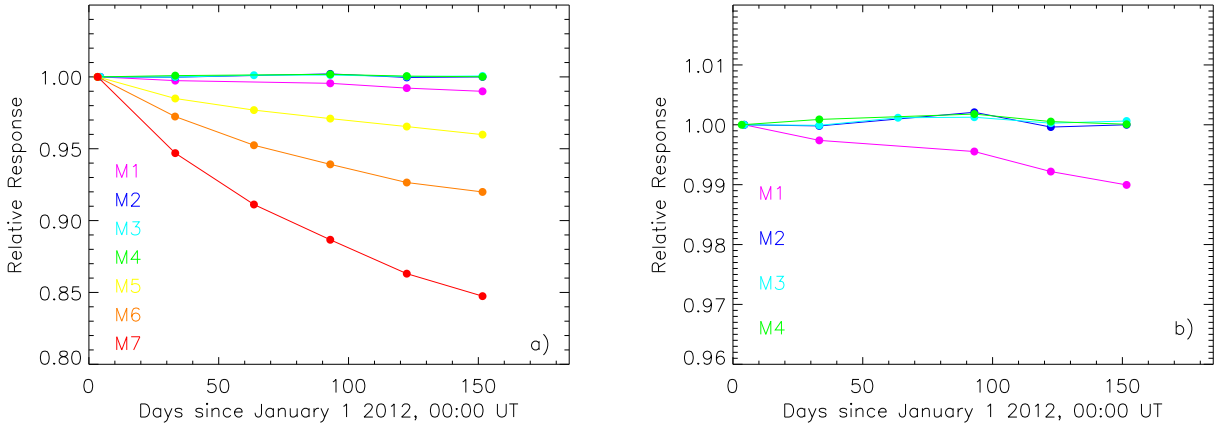

Figure 7. **Lunar Calibration Time Series.** a) The series for bands M1–M7. b) The series for bands M1–M4.

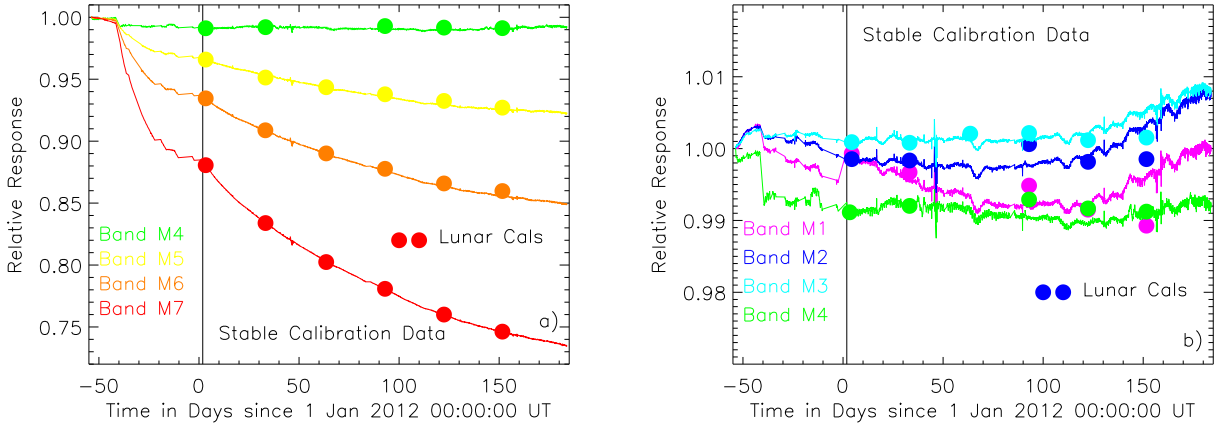

Figure 8. **Solar and Lunar Calibration Comparison.** a) Comparisons for bands M4–M7. b) Comparisons for bands M1–M4. The lunar calibrations agree with the solar calibrations for bands M4–M7. The lunar calibrations show that bands M1–M3 are over-corrected for the diffuser BRDF drift.

comparison of lunar and solar radiometric trends over time. The radiometric trends for bands M4–M7 are in good agreement. The band M4 trends in Fig. 8b show the level of observational noise in these comparisons. For Band M1 the lunar data shows the expected decrease in response over time, while the solar data shows an increase in response during the latter part of the mission. The lunar data shows little change in the response of bands M2 and M3, while the solar data again shows an increase in response during the latter part of the mission. Comparison of the lunar and solar trends for bands M1–M3 is consistent with the SDSM-derived BRDF corrections for these bands over-correcting the F-factor time series, as was discussed in the previous section of the paper. Fig. 9 shows the differences in the lunar and solar calibrations over time; the main disagreement occurs for bands M1–M3 during the latter part of the mission. The lunar trends are consistent with the solar trends where the F-factors are corrected by the normalized H-factors. This observations confirms that the BRDF correction is necessary for the F-factors and that the Channel 8 normalization is necessary for the H-factors.

In a further combination of the lunar and solar calibration time series, the VOST used the F-factors at the time of each lunar calibration to correct the lunar data for the radiometric response of the instrument. These "calibrated" lunar residuals were then averaged over the mission to compute the average bias between VIIRS and the ROLO model for each band. Fig. 10 shows these calibration biases, along with the biases relative to the ROLO model for SeaWiFS, Terra MODIS, and Aqua MODIS derived by Eplee *et al.*[10] The small standard deviation in the mean of the bias for each band shows the agreement in the change in response seen by the

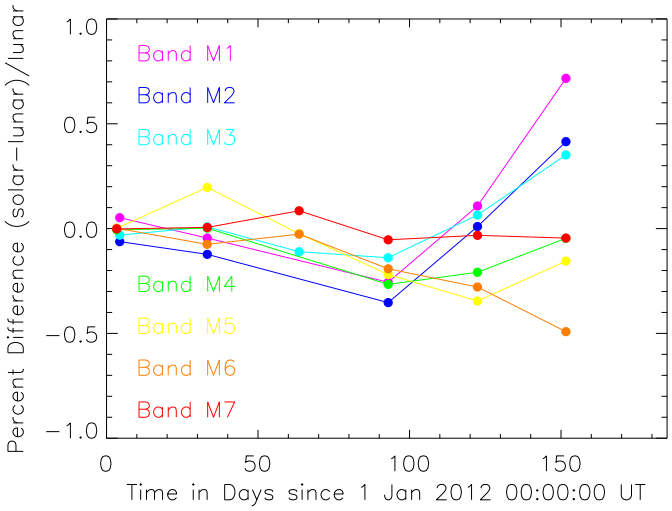

Figure 9. **Solar and Lunar Calibration Differences.** The response differences over time.

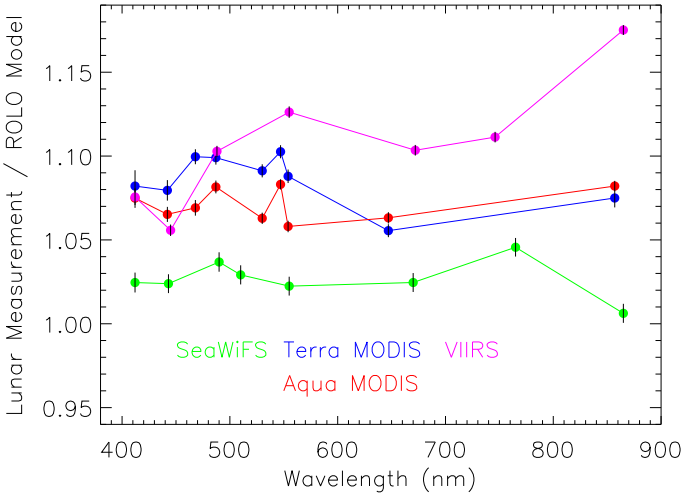

Figure 10. **VIIRS Calibration Relative to MODIS / SeaWiFS.** The VIIRS calibration bias relative to the ROLO Model, compared to the biases of SeaWiFS, Aqua MODIS, and Terra MODIS.

lunar and solar calibrations since the first lunar calibration. However, comparison between VIIRS and the two MODIS instruments for bands above 500 nm wavelength raises the question of the absolute calibration of VIIRS on January 2. This topic will be discussed further in path forward section of the paper.

4. STRIPING CORRECTIONS

The VOST has used the prelaunch calibration and the on-orbit lunar and solar calibrations to derive the calibration for VIIRS over time. This approach has treated each detector within each bands separately, yielding four calibrations of the instrument (for each gain and mirror side). The prelaunch counts-to-radiance coefficients were derived for each detector. The solar-derived instrument response (the F-factors) were derived for each detector. The SDSM-derived corrections for the diffuser BRDF are computed for each band, independent of gain and mirror side. The lunar calibrations are restricted to high gain data and the resulting corrections are computed for each band. This calibration methodology does not mitigate any detector-to-detector striping or

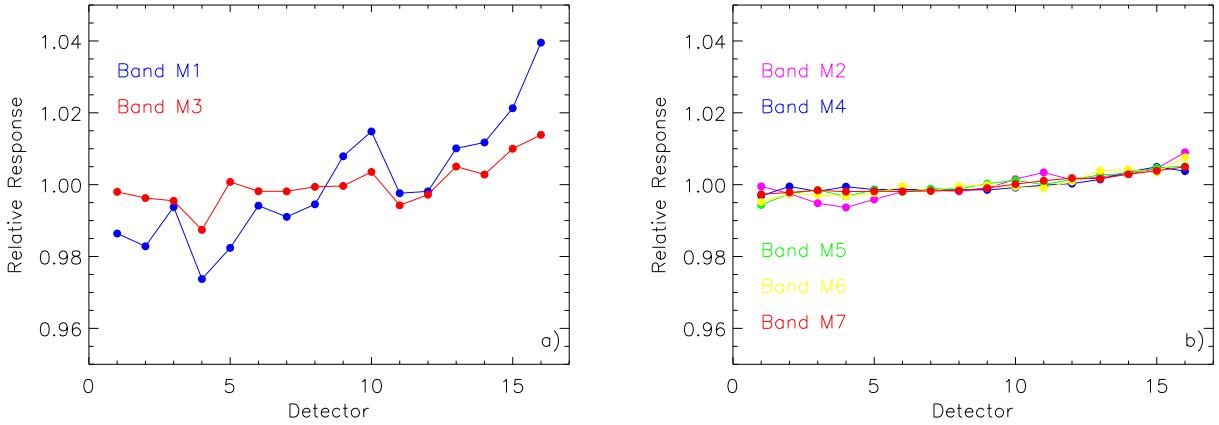

Figure 11. **Detector Relative Response.** a) Responses for Bands M1 and M3. b) Responses for Bands M2 and M4–M7. Bands M1 and M3 show the largest change in response across the detectors.

mirror side-to-mirror side banding in the data products. The VOST has derived a set of striping and banding corrections based on the solar calibration data set.

4.1 Detector Relative Response

Variations in detector response across a band can give rise to striping in ocean color products. To mitigate this striping, the VOST computes a correction for relative detector response across each band. For each solar calibration, the F-factor for each detector is normalized to the mean F-factor for that band, yielding the detector response for the band and solar calibration. To date the relative responses for each band are stable over time, so the responses are averaged for the mission. Fig. 11 shows the detector responses for bands M1–M7. The detectors for bands M1 and M3 show the largest variation across the band. These relative detector response corrections are incorporated into the F-factor production lookup tables. Currently, the VOST computes a single correction for the detector response across each band. Additional corrections will be computed and applied if and when the instrument's on-orbit performance requires it.

4.2 Mirror Side Relative Response

Variations in the mirror side response for a band can give rise to banding in the ocean color data. To mitigate this banding, the VOST computes a correction for the mirror side differences from solar calibration data that has had the relative detector response corrections applied. For each solar calibration, the F-factor for each mirror side is normalized to the mean F-factor of the two mirror sides, yielding the mirror side response for the band and solar calibration. To date the mirror side responses for each band are stable over time, so the responses are averaged for the mission. Fig. 12 shows the mirror side responses. These mirror side corrections are incorporated into the F-factor production lookup tables. Currently, the VOST computes a single correction for the relative mirror side response for each band. Additional corrections will be computed and applied if and when the instrument on-orbit performance requires it.

Incorporation of the detector response corrections and the mirror side response corrections into the production F-factor lookup tables have substantially reduced the striping and banding in the VIIRS ocean color data products.[11] Fig. 13 shows the effect of these corrections on ocean color chlorophyll products.

5. VICARIOUS CALIBRATION

As was discussed in the introduction, the vicarious calibration of VIIRS against *in situ* measurements performs the spectral calibration of the instrument. This early in the mission, the vicarious calibration procedure for ocean color data from VIIRS is:

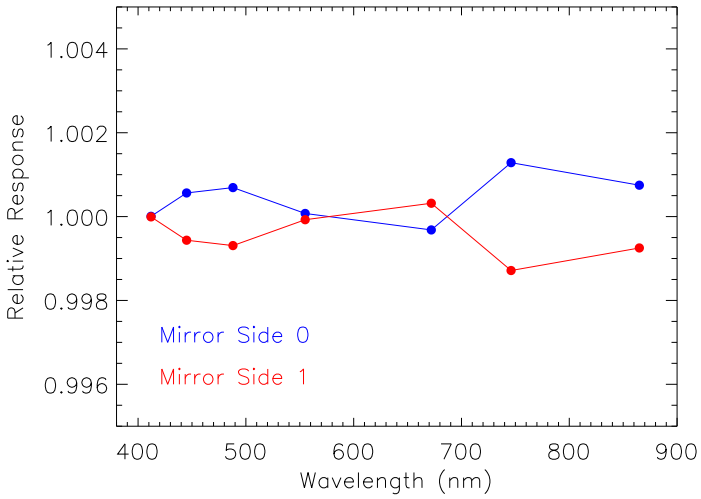

Figure 12. **Mirror Side Relative Response.** The response for bands M1–M7.

Table 3. **Vicarious Gains and Lunar Bias.** The vicarious gains and lunar calibration biases relative to the ROLO model. [a]Assumed.

Band	**Wavelength (nm)**	**Vicarious Gain**	**Lunar Bias**
M1	412	0.9767	1.0770
M2	445	1.0202	1.0547
M3	488	1.0273	1.1021
M4	555	0.9936	1.1252
M5	672	1.0257	1.1029
M6	746	1.0470	1.1103
M7	865	1.00[a]	1.1743

1) The calibration of Band M7 (865 nm) is assumed to be correct. The M7 gain can be off by $\sim 5\%$ without introducing a significant error into the vicarious calibration.[12,13]

2) Band M6 (746 nm) is calibrated relative to Band M7 so the atmospheric correction algorithm retrieves the expected aerosol types and optical depths for open ocean scenes.

3) TOA radiances computed for the bands M1–M5 are calibrated against an ocean surface reflectance model, where the surface reflectances are propagated to the top of the atmosphere using the retrieved atmospheric correction parameters.[8]

The ocean surface reflectance model-based vicarious calibration does not provide as accurate a calibration in the blue as does the calibration against MOBY,[8] so when a sufficient number of satellite/MOBY matchups become available for VIIRS, the model-based calibration will be replaced with the calibration against MOBY. Vicarious calibration should yield the optimum water-leaving radiances for the sensor/algorithm system-level calibration. If the prelaunch spectral calibration of VIIRS is accurate, vicarious gains should be of order unity. Table 3 provides the vicarious gains, along with the ROLO-derived lunar calibration biases. Fig. 14 also shows the vicarious gains.

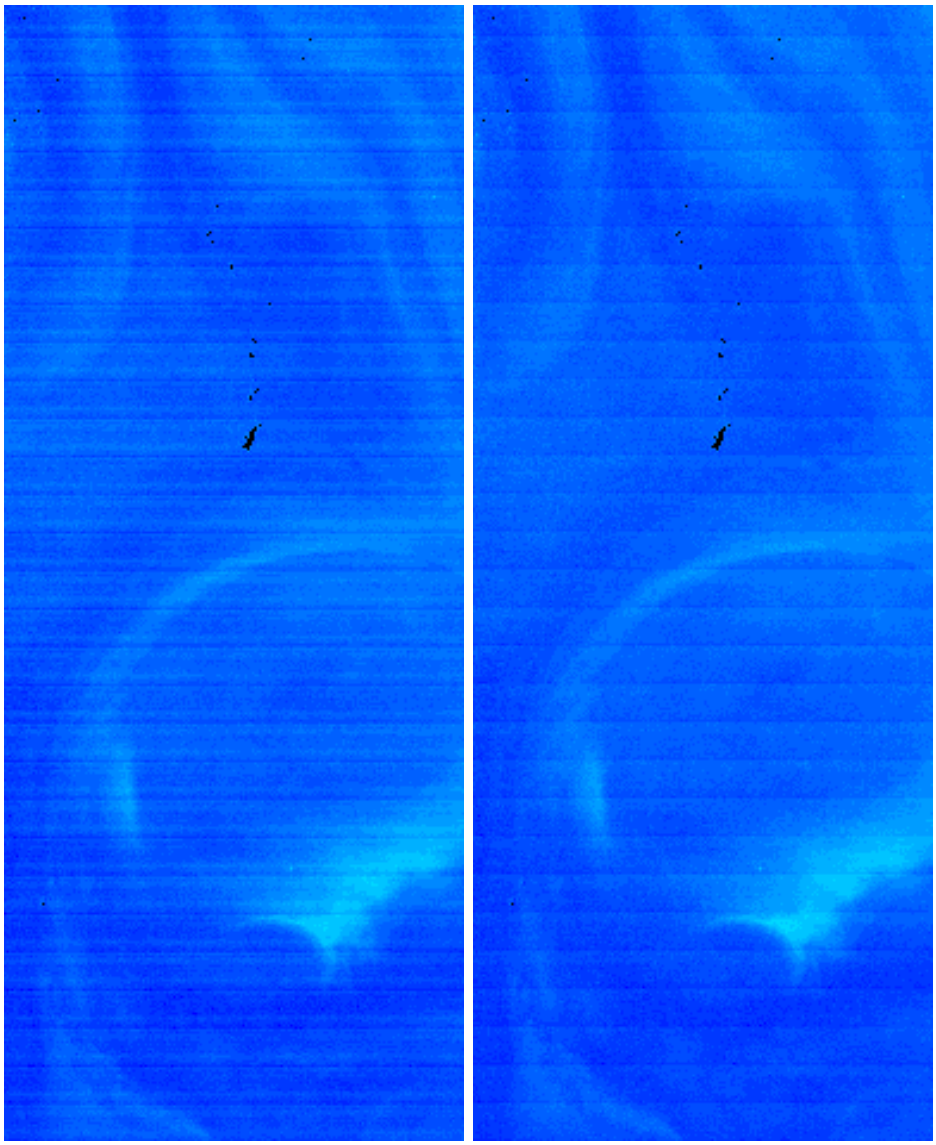

Figure 13. **Striping and Banding Correction.** VIIRS chlorophyll images off of the U.S. mid-Atlantic coast obtained on May 31, 2012. a) The original image. b) The image processed with striping and banding corrections. There are still residual gradients in the corrected image.

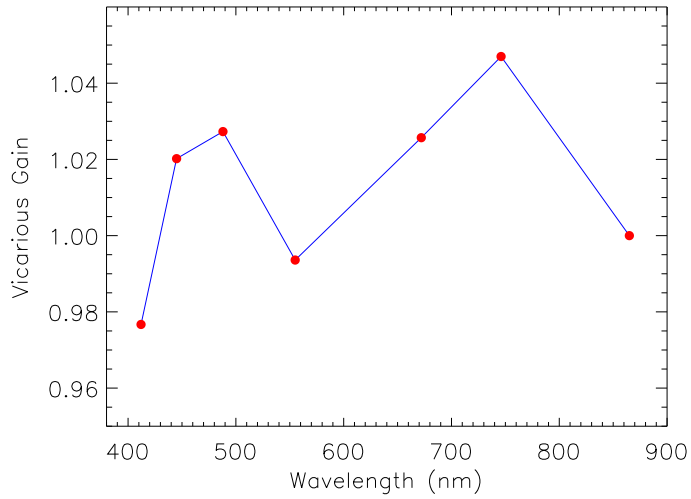

Figure 14. **VIIRS Vicarious Gains.** The model-based vicarious gains.

6. THE PATH FORWARD

This paper presents the current understanding of the on-orbit calibration of VIIRS by the NASA VIIRS Ocean Science Team. The VOST has drawn on its experience with SeaWiFS and MODIS to derive a relatively robust calibration of VIIRS for ocean color data processing within 8 months of the Suomi NPP satellite launch. The current status of the on-orbit solar, lunar, and vicarious calibration allows the VOST to begin its assessment of the VIIRS ocean color data products.[11] There are a number of issues with the VIIRS calibration that the VOST is currently investigating.

Fig. 15 shows the current spectral calibration of VIIRS by the VOST. The blue line shows F-factors computed from the first solar calibration. The green line shows vicarious gains derived from the model ocean surface reflectance. The red line shows the inverse of the ROLO residuals (ROLO/VIIRS). The VOST is investigating possible normalizations of the F-Factors at the first calibration. This addition to the on-orbit spectral calibration should bring the ROLO residuals closer to unity and should decrease the amplitude of the vicarious gains. The overall impact on the ocean color data products would be negligible due to the vicarious calibration.

Other open calibration issues include:

1) The SDSM-derived BRDF corrections for channels 1–3 over-correct the F-factors for bands M1–M3. The BRDF corrections are required for the F-factor trends to agree with the lunar trends. How should the BRDF-correction be modified for the blue bands? Lunar calibrations may be required to supplement the F-factors computed for these bands.

2) The absolute value of the F-factors at the time of the first lunar calibration (January 2, 2012) is uncertain. The current value is determined by normalizing the time series to the first light observation. Is there a better way to calibration the F-factors on this date?

3) Lunar observations are currently averaged over the detectors in each band. Is the noise in the lunar time series sufficiently low to allow a per-detector calibration? Such a calibration would take the *ith* detector scan lines from the lunar image sequence (see Fig. 6) to form a single oversampled lunar image. Per-detector calibration for MODIS had marginal quality with 10 detectors per band. The 16 detectors per band for VIIRS presents a greater challenge.

4) Is a more rigorous striping/banding correction required for the ocean color products?

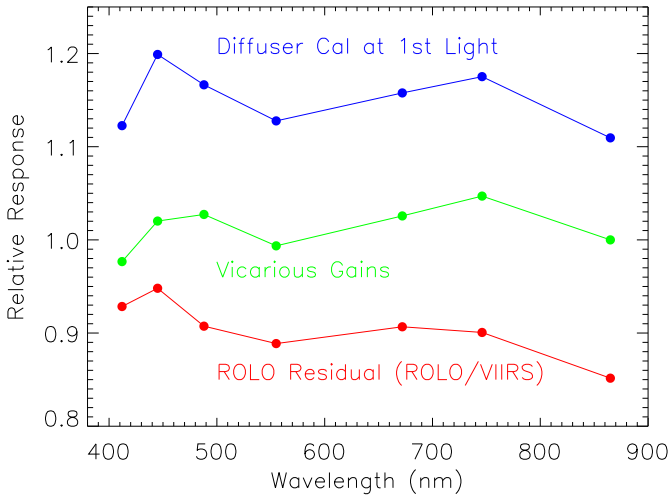

Figure 15. **VIIRS Spectral Calibration.** Comparison of the absolute solar diffuser calibration at first light, the lunar residuals from the ROLO model, and the vicarious gains. The spectral dependence of these parameters is tied to the spectral calibration of the instrument.

5) A robust vicarious calibration of VIIRS against MOBY should yield more accurate vicarious gains for the blue bands.

The VOST will be addressing these issues over the next year to optimize the ocean color data products that can be produced from VIIRS data.

REFERENCES

[1] National Research Council, *Assessing Requirements for Sustained Ocean Color Research and Operations*, The National Academies Press, Washington, D.C. (2011).

[2] F.J. De Luccia, D.I. Moyer, E.H. Johnson, K.W. Rausch, N. Lei, K. Chiang, X. Xiong, E.M. Haas, J. Fulbright, and G. Iona, "Discover and characterization of on-orbit degradation of the VIIRS rotating telescope assembly," in *Earth Observing Systems XVII*, J.J. Butler, X Xiong, and X. Gu, eds., *Proc. SPIE* **8510**, 85101B, (2012).

[3] H.H. Kieffer and T.C. Stone, "The spectral irradiance of the Moon," *Astron. J.* **129**, 2887–2901 (2005).

[4] T.C. Stone and H.H. Kieffer, "Use of the Moon to support on-orbit sensor calibration for climate change measurements," in *Earth Observing Systems XI*, J.J. Butler and J. Xiong, eds., *Proc. SPIE* **6296**, 62960Y (2006).

[5] D.K. Clark, H.R. Gordon, K.J. Voss, Y. Ge, W. Broenkow, and C. Trees, "Validation of atmospheric correction over the oceans," *J. Geophys. Res.* **99**, 7293–7307 (1997).

[6] D.K. Clark, M.E. Feinholz, M.A. Yarbrough, B.C. Johnson, S.W. Brown, Y.S. Kim, and R.A. Barnes, "Overview of the radiometric calibration of MOBY," in *Earth Observing Systems VI*, W.L. Barnes, ed., *Proc. SPIE* **4483**, 64–76 (2002).

[7] B.A. Franz, S.W. Bailey, P.J. Werdell, and C.R. McClain, "Sensor-independent approach to the vicarious calibration of satellite ocean color radiometry," *Appl. Opt.* **46**, 5068–5082 (2007).

[8] P.J. Weredell, S.W. Bailey, B.A. Franz, A. Morel, and C.R. McClain, "On-orbit vicarious calibration of ocean color sensors using an ocean surface reflectance model." *Appl. Opt.* **46**, 5649-5666 (2007).

[9] F.S. Patt, R.E. Eplee, R.A. Barnes, G. Meister, and J.J. Butler, "Use of the Moon as a calibration reference for NPP VIIRS," in *Earth Observing Systems X*, J.J. Butler, ed., *Proc. SPIE* **5882**, 588215 (2005).

[10] R.E. Eplee, Jr., J.-Q. Sun, G. Meister, F.S. Patt, X. Xiong, and C.R. McClain, "Cross calibration of SeaWiFS and MODIS using on-orbit observations of the Moon," *Appl. Opt.* **50**, 120–133 (2011).

[11] K.R. Turpie, B.A. Franz, C.R. McClain, W.D. Robinson, R.E. Eplee, Jr., G. Meister, G.F. Fireman, F.S. Patt, and R.A. Barnes, "Suomi NPP VIIRS ocean color data product early mission assessment," in *Earth Observing Systems XVII* J.J. Butler, X Xiong, and X. Gu, eds., *Proc. SPIE* **8510**, 85101I, (2012).

[12] H.R. Gordon, "In-orbit calibration strategy for ocean color sensors," *Remote Sens. Environ.* **63**, 265–278 (1998).

[13] M. Wang and H.R. Gordon, "Calibration of ocean color scanners: how much error is acceptable in the near infrared?," *Remote Sens. Environ.* **82**, 497–504 (2002).